Materials Advances

ROYAL SOCIETY OF CHEMISTRY

PAPER

View Article Online
View Journal | View Issue

Cite this: *Mater. Adv.*, 2025, 6, 6291

Revealing an efficient copper oxide nanoparticle catalyst for the reduction of the hazardous nitrophenol: experimental and DFT studies

Elsayed Elbayoumy, *[a] Emadeldin M. Ibrahim,[b] Ashraf El-Bindary,[a] Tamaki Nakano [cd] and Mohamed M. Aboelnga [ae]

The accumulation of hazardous nitrophenols generated from industrial wastewater necessitates every possible scientific collaboration to help protect our ecosystem. To participate in this increasingly pressing matter, we provide a synthesized crosslinked vinyl polymer loaded with copper oxide nanoclusters as a high-performance catalyst for the reduction of 4-nitrophenol to 4-aminophenol. The catalyst was synthesized *via* free radical polymerization using divinylbenzene (DVB) as the monomer. The resulting polymer served as a support matrix for copper oxide nanoparticles (CuO NPs). The structural characteristics of the synthesized composites were analyzed for their properties using FTIR, TGA, XRD, TEM, and BET for surface area measurements. The results confirm that copper oxide nanoparticles (CuO NPs) were uniformly distributed across the poly(DVB) surface with no aggregation. BET analysis revealed a microporous structure with a defined surface area of 90.0928 m^2 g^{-1}. When employed as a heterogeneous catalyst in the hydrogenation of 4-nitrophenol (4-NP), the composite achieved a reaction rate constant of 0.45 min^{-1} and a half-life of 1.45 min. Notably, the catalyst could be easily recovered from the reaction mixture and reused for four consecutive cycles without significant loss in activity. DFT calculations were carried out to elucidate the underlying reduction mechanism of nitrophenol.

Received 10th June 2025,
Accepted 27th July 2025

DOI: 10.1039/d5ma00620a

rsc.li/materials-advances

1. Introduction

The accelerated expansion of industrial activities and contemporary technology has increased the reliance on organic compounds for synthesizing commercially significant materials.[1,2] Notably, 4-nitrophenol (4-NP), a basic aromatic molecule, is widely employed as a precursor in industries such as textiles, dyes, explosives, pharmaceuticals, pesticides, paper, and petroleum refining.[3–6] This widespread use has resulted in the environmental accumulation of toxic byproducts, posing substantial risks to ecosystems, humans, and wildlife.[7] Owing to its toxicity, carcinogenicity, and high water solubility, 4-NP is a prominent aquatic pollutant, implicated in adverse health effects, including headaches, nausea, cyanosis, abdominal pain, hepatorenal dysfunction, and neurological disorders.[8–15] In addition, it is known to cause fatal diseases in animals.[16–18] Thus, addressing the environmental and health risks associated with 4-NP has become a critical focus of research, attracting considerable attention recently. Various methods have been explored to eliminate 4-NP from water, including hydrogenation,[19–21] catalytic amination, photocatalytic degradation,[21] adsorption,[22] ozonation,[23] biodegradation,[24] and electrochemical methods.[25] However, conventional approaches suffer from limitations, such as lengthy processing times, elevated cost, suboptimal efficiency, stringent reaction conditions, and the generation of harmful aromatic byproducts.[26,27] In contrast, the catalytic reduction of 4-nitrophenol (4-NP) into 4-aminophenol (4-AP) provides a safer alternative with minimal toxicity. This method is particularly advantageous, owing to its rapid reaction kinetics, cost-effectiveness, and exceptional catalytic performance relative to existing strategies.[28,29] Metal nanoparticles, characterized by their extensive surface area relative to volume and distinct physicochemical properties in comparison to bulk materials, are pivotal in diverse applications.[30–34] Nanoparticles of metals, including silver,

[a] *Chemistry Department, Faculty of Science, Damietta University, New Damietta 34517, Egypt. E-mail: sayedelbayoumy@du.edu.eg, abindary@du.edu.eg, mohamed-aboelnga@du.edu.eg*
[b] *Chemistry Department, Faculty of Science, Mansoura University, Dakahlia 35516, Egypt. E-mail: mmemadeldin@outlook.com*
[c] *Institute for Catalysis and Graduate School of Chemical Sciences and Engineering, Hokkaido University, N21 W10, Kita-ku, Sapporo 001-0021, Japan. E-mail: tamaki.nakano@cat.hokudai.ac.jp*
[d] *Integrated Research Consortium on Chemical Sciences (IRCCS), Institute for Catalysis, Hokkaido University, N21 W10, Kita-ku, Sapporo 001-0021, Japan*
[e] *King Salman International University, Faculty of Basic Sciences, Ras Sudr, 46612, South Sinai, Egypt*

copper, iron, palladium, cobalt, nickel, gold, and platinum, have been successfully employed as catalysts for degrading toxic organic pollutants.[35–43]

Currently, nanostructured particles (NPs) have garnered significant attention in catalytic processes due to their distinctive electronic properties and large surface areas.[44–47] Among these, copper oxide (CuO) nanoparticles stand out as highly efficient catalysts for various chemical reactions, such as dimethyldichlorosilane synthesis,[48] ring-opening reactions,[49] and dye degradation.[50] However, as a result of their extensive surface area and elevated surface energy, CuO NPs are prone to instability and self-aggregation, which can lead to a reduction in catalytic efficiency, as catalytic activity is closely linked to surface area. To overcome this challenge, CuO NPs are typically loaded onto supporting matrices[51–53] or synthesized into specific structures, such as flower-like microspheres,[54] urchins,[55] or hollow nanospheres.[56] However, these specialized structures often require complex modification and preparation processes. Moreover, the catalytic characteristics of CuO NPs may be diminished when they are embedded into supports, as the supporting matrices often possess relatively limited surface area, limiting the availability of catalysts to interact with reactants. As a result, the development of novel supporting materials for CuO NPs remains a critical area of scientific research to fully harness their catalytic potential.

Inorganic supports functionalized with metal nanoparticles, while effective, exhibit constrained structural adaptability.[57] Conversely, porous organic polymers enable greater structural versatility, as their synthesis from diverse monomers permits tailored designs. The integration of functional groups within the polymer framework further enhances interactions with metal nanoparticles, minimizing leaching and preserving catalytic efficiency.[58] For instance, poly(divinylbenzene) (poly(DVB)), a hyper-crosslinked vinyl-based polymer, is synthesized *via* free radical polymerization of divinylbenzene, offering a cost-effective route. It offers several advantages as a porous organic support, such as facile synthesis, affordability, high surface area, and robust thermal/chemical stability.[59] Earlier research reported a poly(DVB)-supported palladium nanoparticle catalyst for oxidizing benzyl alcohol to benzaldehyde and toluene. This system exhibited no detectable palladium leaching into the reaction medium and retained activity over five reuse cycles after a facile filtration-based recovery.[31]

Recent studies have explored green-synthesized metal oxide nanoparticles using plant-based extracts for environmental remediation, combining catalytic efficacy with sustainable production methods.[60–62] Despite the promising use of green-supported catalysts, such as metal biopolymer composites and green-synthesized metal oxide systems, their broader application is often hindered by critical limitations. These include insufficient thermal and chemical stability, leaching of active metal sites into the reaction medium, and complicated synthesis procedures that can impact reproducibility. In contrast, porous organic polymers, such as poly(DVB), provide a structurally tunable, thermally robust, and chemically inert framework that enables uniform nanoparticle dispersion and efficient catalysis. The CuO/poly(DVB) system proposed in this study addresses these shortcomings by offering a cost-effective, reusable, and highly active platform for the catalytic reduction of 4-nitrophenol (4-NP).[63] Furthermore, the facile synthesis of poly(DVB) and its high surface area facilitate better accessibility of active sites, while minimizing the aggregation commonly observed in unsupported or biopolymer-supported CuO nanoparticles. These advantages make CuO/poly(DVB) a competitive and scalable alternative for environmental remediation applications.

In this work, a CuO/poly(DVB) composite was fabricated as a heterogeneous catalyst in two stages: (1) poly(DVB) synthesis *via* AIBN-initiated free radical polymerization of divinylbenzene in acetonitrile, and (2) subsequent CuO nanoparticle immobilization onto the polymer matrix (Fig. 1). The catalytic performance of the composite was evaluated for its efficacy in reducing toxic nitrophenol to aminophenol. Complementary DFT simulations revealed atomistic insights into the reaction mechanism, highlighting intermediate species, and deepening mechanistic understanding.

2. Materials and methods

2.1. Materials

α,α′-Azobisisobutyronitrile (AIBN), acetonitrile, and sodium borohydride were acquired from Wako Chemical (Osaka, Japan).

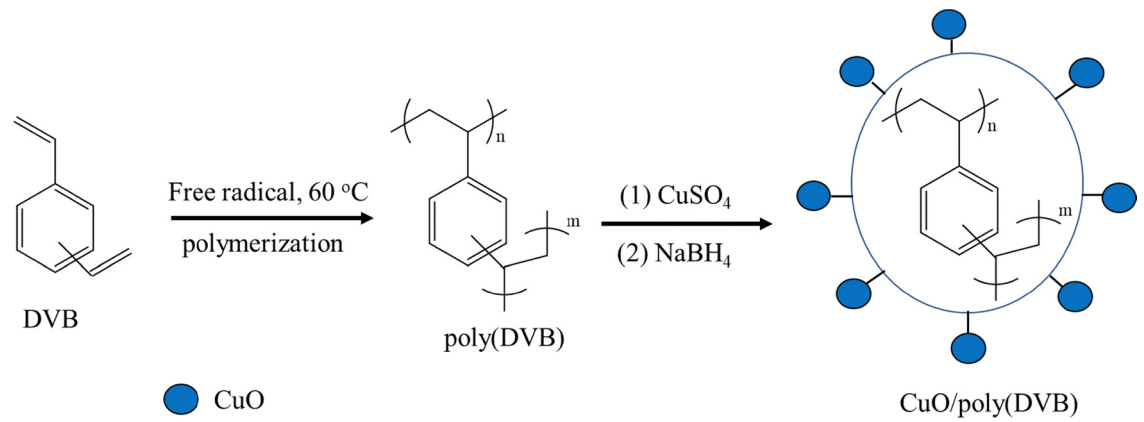

Fig. 1 Schematic representation for the preparation of poly(DVB) and CuO/poly(DVB).

AIBN was synthesized using ethanol, and acetonitrile was distilled prior to use. Divinylbenzene (DVB) was sourced from TCI (Tokyo, Japan) and used directly without additional purification. Nitrophenol and copper(II) sulfate pentahydrate were obtained from MilliporeSigma (formerly Sigma-Aldrich; St. Louis, MO, USA) and used as received without further processing. High-grade methanol was employed without purification. Deionized water was employed throughout the experiments.

2.2. Synthesis of poly(DVB)

Poly(divinylbenzene) (poly(DVB)) was prepared using a method detailed in our previous study.[31] This involved the free radical polymerization of divinylbenzene (DVB) with α,α′-azobisisobutylonitrile (AIBN) as the initiator and acetonitrile as the solvent. Specifically, AIBN (0.7435 g, 4.79 mmol) was introduced into a 300 mL round-bottom flask with two necks, which was equipped with a condenser. The flask was subsequently evacuated and purged with nitrogen gas three times. Acetonitrile (175 mL) and DVB (14.24 mL, 0.1 mol) were then introduced into the flask under stirring to create a uniform solution. The reaction mixture was maintained at 60 °C under an N_2 atmosphere for 24 h. Following completion, it was allowed to cool to room temperature. The poly(DVB) product was collected by means of centrifugation and thoroughly rinsed with methanol and acetone to remove any unreacted monomers or residual initiators. After purifying the polymer, it was vacuum-dried for 24 h, providing 10.154 g (78% yield) of poly(DVB) as a white powdered solid.

2.3. Preparation of CuO nanoparticle–polymer composite

The copper oxide nanoparticle–polymer composite was synthesized in air by reducing copper(II) sulfate pentahydrate ($CuSO_4 \cdot 5H_2O$) with sodium borohydride ($NaBH_4$)in the presence of synthesized poly(DVB), following a modified version of a previously described method.[64] Specifically, 0.3 g of poly(DVB) was stirred in 25 mL of a methanol solution containing $CuSO_4 \cdot 5H_2O$ (17.16 mM, constituting 10% of the polymer mass) for 1 h to thoroughly load Cu^{2+} ions into the poly(DVB) framework. Following the immersion period, the Cu^{2+}/poly(DVB) complex was isolated from the unreacted $CuSO_4 \cdot 5H_2O$ solution by centrifugation and thoroughly rinsed with methanol to eliminate residual copper sulfate. The complex was subsequently chemically reduced under ambient conditions by introducing 10 mL of a freshly prepared $NaBH_4$ methanol solution (1.11 mM) and stirring for 1 h to yield the CuO/poly(DVB) composite. The final product was separated *via* centrifugation, rinsed with methanol, dried, and stored under vacuum until characterization.

2.4. Catalytic reduction of nitrophenol

The catalytic activity of the CuO nanoparticles/poly(DVB) composite was evaluated through the hydrogenation of 4-nitrophenol (4-NP) to 4-aminophenol (4-AP) as a representative reaction. Adopting literature protocols,[65–67] a freshly prepared 10 mM $NaBH_4$ solution (5 mL) was combined with 5 mL of a 1 mM 4-NP solution. Subsequently, 20 mg of the CuO/poly(DVB) catalyst was added to the mixture, which was then diluted to 50 mL with deionized water. Aliquots (2 mL) were collected every 2 min through a nylon syringe filter (0.22 μm) to remove particulates and characterized by UV-vis spectroscopy (250–500 nm). Reaction progress was monitored *via* the decay of the 400 nm absorption band (characteristic of 4-NP) and the visual color transition from yellow (4-nitrophenol) to colorless (4-aminophenol).

2.5. Characterization techniques

A JASCO FT/IR-6100 spectrometer was used to obtain Fourier-transform infrared (FTIR) spectra, with samples prepared as potassium bromide (KBr) pellets. Thermogravimetric analysis (TGA) was carried out on a Rigaku Thermo plus TG8120 instrument under a nitrogen flow of 20 mL min^{-1}, and heating at 10 K min^{-1} from room temperature to 750 K in an aluminum crucible. Transmission electron microscopy (TEM) images were captured using a ThermoFisher Talos L120C G2 microscope. Wide-angle X-ray diffraction (XRD) patterns were recorded on a Siemens D-500 diffractometer with Cu Kα radiation (λ = 1.54 Å). Surface area and pore size distribution were determined by nitrogen physisorption at 77 K using a Quantachrome analyzer (USA), employing the Brunauer–Emmett–Teller (BET) method. UV-vis absorption spectra were recorded using a Jasco V-630 spectrophotometer with a 1 cm quartz cuvette in the range of 250–500 nm.

2.6. Computational methods

To explore the potential intermediates involved in the reaction mechanism on the CuO cluster, density functional theory (DFT) calculations were performed using the B3LYP functional, as implemented in Gaussian. Relevant studies support the use of this functional in such systems.[68–70] In this study, two basis sets were applied: initially, the B3LYP/cc-pVDZ basis set was used to optimize the geometry of the CuO nanocluster. Following that, the 6-31G(d) basis set was employed for subsequent reaction steps. The use of B3LYP/cc-pVDZ for geometric optimization of CuO nanoclusters has been successfully reported in previous work.[71] Moreover, the B3LYP functional in combination with the 6-31G(d) basis set has been widely and successfully applied in treating various metal-containing systems.[72–75]

The CuO cluster model was selected based on previous research, which identified the Cu_nO_m configuration, with a ratio of approximately 2 : 1, as the most stable form ref. 71. Therefore, a Cu_6O_3 cluster was used as the representative model in the current work. The chemical model includes the adsorption of a nitrophenol compound onto the Cu_6O_3 cluster, and the reaction mechanism follows the pathway briefly illustrated in Scheme 1. This mechanism proceeds through different consecutive steps, ultimately leading to the formation of the reduced product, aminophenol. An alternative six-step mechanism was also identified, where protonation of nitrogen occurs before the elimination of the second oxygen atom as a water molecule. All intermediates were comprehensively analyzed, with their identification as local minima or transition states verified through vibrational frequency calculations at the same theoretical level as that used for geometric optimization. To elucidate the electronic interactions between phenol derivatives

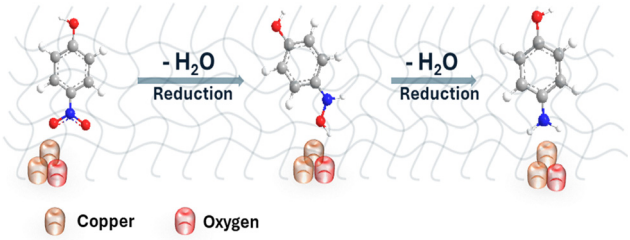

Scheme 1 Proposed mechanism for the catalytic hydrogenation of nitrophenol mediated by a CuO nanoparticle catalyst.

and the Cu_6O_3 cluster, the frontier molecular orbitals, specifically the highest occupied molecular orbital (HOMO) and the lowest unoccupied molecular orbital (LUMO), were examined to assess charge transfer processes.

3. Results and discussion

3.1. FTIR analysis

Fig. 2 displays the FTIR spectra of poly(DVB) and the CuO/poly(DVB) composite. For poly(DVB), four distinct absorption bands appear between 1447 and 1697 cm^{-1}, assigned to aromatic C=C stretching vibrations. Vibrational modes corresponding to aliphatic C–H groups are observed in the 2900–3017 cm^{-1} range. A peak at 712 cm^{-1} arises from out-of-plane deformation vibrations of the aromatic ring, while symmetric and asymmetric out-of-plane deformation modes of adjacent hydrogen atoms, evident at 796 and 834 cm^{-1}, confirm the di-substituted benzene ring structure. Absorption bands at 901 and 992 cm^{-1} correspond to vinyl group vibrations.[76–78] Upon incorporation of CuO nanoparticles, two new peaks emerge in the composite spectrum at 619 cm^{-1} and 1123 cm^{-1}, which are not present in the spectrum of poly(DVB). These are assigned to Cu–O stretching vibrations, indicating successful anchoring of monoclinic copper oxide nanoparticles onto the polymer matrix. The presence of these additional peaks, along with a minimal shift in the original polymer bands, suggests that CuO nanoparticles are well dispersed without disrupting the polymer backbone.[79]

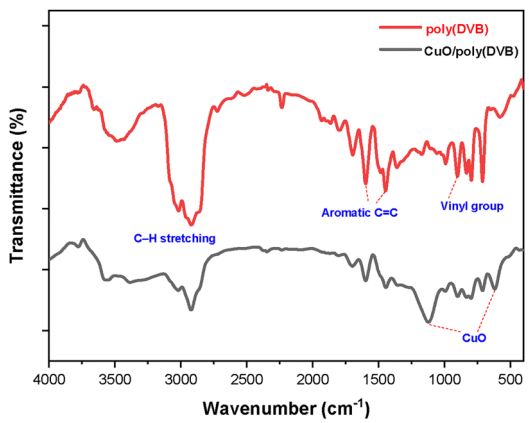

Fig. 2 FTIR spectra of poly(DVB) and CuO/poly(DVB).

3.2. Thermal gravimetric analysis

Fig. 3A displays the thermogravimetric analysis (TGA) and derivative thermogravimetric analysis (DTG) profiles for the CuO/poly(DVB) composite. The TGA curve indicates three primary degradation stages, occurring within the temperature ranges of 278.17 °C–372.24 °C, 372.24 °C–495.30 °C, and 495.30 °C–674.77 °C, with corresponding weight losses of 11.71%, 30.87%, and 24.47%, respectively. The DTG curve shows three distinct peaks, with the highest degradation rates observed at temperatures of 346.70 °C, 418.92 °C, and 571.40 °C for stages 1 through 3. All the degradation stages are assigned to the decomposition of the polymer backbone in the CuO/poly(DVB) composite, a finding that aligns with observations in previous studies.[80–82] The activation energy (E^*) for the three main thermal degradation stages of the CuO/poly(DVB) composite was determined using the Coats–Redfern method.[83,84] For a first-order degradation process, the relationship between the decomposed sample fraction (α), temperature (T), and heating rate (θ) is described by eqn (1):

$$\log\left[\frac{-\log\log(1-\alpha)}{T^2}\right] = \log\log\left[\frac{A'R}{\theta E^*}\left(1-\frac{2RT}{E^*}\right)\right] - \frac{E^*}{2.303RT} \quad (1)$$

where A' represents the Arrhenius constant, and R denotes the universal gas constant. The parameter α is calculated using the initial sample mass (W_0), the residual mass after degradation (W_f), and the mass at a specific temperature (W_t), as expressed in eqn (2):

$$\alpha = \frac{W_o - W_t}{W_o - W_f} \quad (2)$$

By applying eqn (1) to the TGA experimental data and plotting the relationship between $\log\left[\frac{-\log\log(1-\alpha)}{T^2}\right]$ and $1/T$, we can determine the values of the activation energy and the Arrhenius constant from the resulting linear plot (see Fig. 3B).

The thermodynamic parameters (ΔS^*, ΔH^*, and ΔG^*) for the three thermal degradation processes of CuO/poly(DVB) were calculated according to eqn (3)–(5).[85,86]

$$\Delta S^* = 2.303R\left[\log\log\left(\frac{A'h}{K_B T}\right)\right] \quad (3)$$

$$\Delta H^* = E^* - RT \quad (4)$$

$$\Delta G^* = \Delta H^* - T\Delta S^* \quad (5)$$

where h symbolizes Planck's constant, and k_B represents Boltzmann's constant. Table 1 compiles the thermal activation energy (E^*), Arrhenius constant, and thermodynamic parameters (ΔG^*, ΔH^*, and ΔS^*) for the thermal decomposition of CuO/poly(DVB). The positive ΔG^* and ΔH^* values confirm that the degradation of the composite across all three stages is thermodynamically non-spontaneous and endothermic.

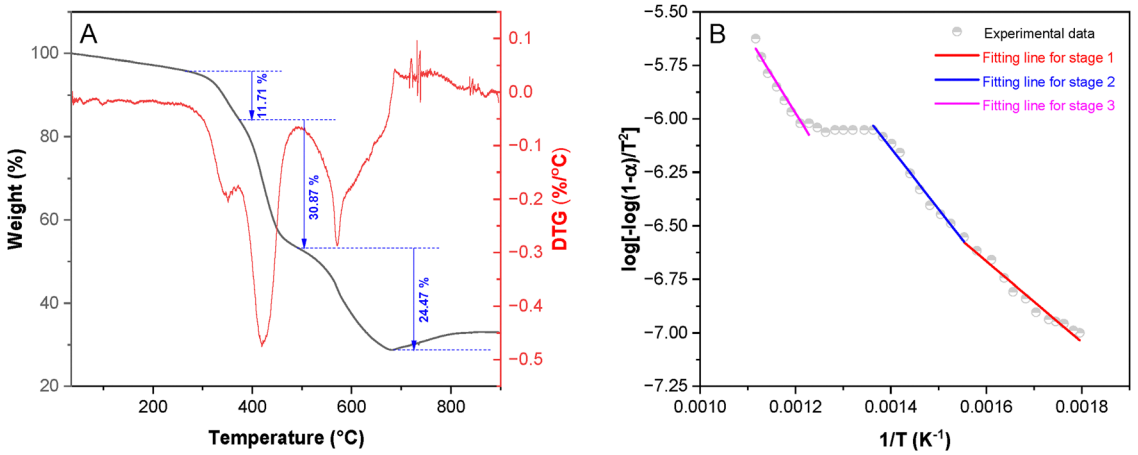

Fig. 3 (A) Thermogravimetric analysis (TGA) and derivative thermogravimetric analysis (DTG) profiles; (B) Coats–Redfern kinetic plot for the CuO/poly(DVB) composite.

3.3. Transmission electron microscopy

The morphological features and particle size distribution of the CuO/poly(DVB) composite were analyzed using transmission electron microscopy (TEM), with the findings illustrated in Fig. 3. The data reveal that CuO/poly(DVB) comprises microsphere particles measuring 2–4 μm, primarily composed of poly(DVB) (Fig. 4a). CuO nanoparticles appear as dark spots on the surface of these spheres (Fig. 4b). Additionally, Fig. 3B confirms that the CuO nanoparticles are well dispersed across the poly(DVB) surface, with no significant aggregation detected. The electron beam diffraction images shown in Fig. 4c reveal distinct bright spots corresponding to the CuO nanoparticles, indicating that these particles are indeed nano-sized crystals. The size distribution of CuO nanoparticles dispersed on the poly(DVB) surface is illustrated in Fig. 4d, indicating an average particle size of approximately 33 nm.

3.4. X-ray diffraction (XRD) analysis

The crystalline structure of the CuO/poly(DVB) catalyst was characterized using X-ray diffraction (XRD), as shown in Fig. 5. The XRD pattern of CuO/poly(DVB) reveals distinct diffraction peaks at 2θ values corresponding to 18.929°, 22.746°, 28.118°, 28.992°, 32.144°, 35.675°, 38.517°, 48.695°, 52.523°, 54.547°, 59.360°, 60.276°, 65.251°, 74.002°. According to the JCPDS (File No. 00-045-0937) card, the diffraction peaks observed in the range of 32.144° to 74.002° can be assigned to the following crystallographic planes of monoclinic CuO nanoparticles: (−110), (002), (111), (−202), (112), (020), (202), (−113), (122), and (004). However, the peaks identified between 18.929° and 28.992° correspond to the polymeric structure of poly(DVB). Similar findings regarding the polymeric structure of DVB have been reported in previous studies.[87,88] This confirms that the CuO/poly(DVB) composite consists of both pure CuO nanoparticles and the organic phase of poly(DVB). The crystallite size of the CuO nanoparticles was calculated from the XRD data using the Scherrer equation:[89,90]

$$D = \frac{K\lambda}{\beta \cos\theta} \quad (6)$$

where D represents the crystallite size (in nm), K is the Scherrer constant (0.89), λ denotes the X-ray wavelength (0.15406 nm), β corresponds to the full width at half maximum (FWHM), and θ is the Bragg angle. Additionally, the CuO nanoparticles exhibit an average crystallite size of approximately 1.541 nm.

3.5. Energy dispersive X-ray spectroscopy (EDS)

To further assess the elemental composition and dispersion of copper oxide in the composite, energy dispersive X-ray spectroscopy (EDS) was performed. As shown in Fig. 6, the EDS spectrum displays characteristic peaks for carbon (C), oxygen (O), and copper (Cu). The measured weight percentages were 44.58% C, 48.13% O, and 7.28% Cu, while the atomic percentages were 54.30% C, 44.02% O, and 1.68% Cu. These results confirm the successful incorporation and uniform distribution of CuO nanoparticles on the poly(DVB) support, corroborating the structural and catalytic stability of the composite observed in other characterization results.

Table 1 Thermal activation energies and thermodynamic parameters for the CuO/poly(DVB) composite

Degradation stage	$E^{\star a}$ (kJ mol^{-1})	A'^{a} (S^{-1})	$\Delta S^{\star b}$ (J mol^{-1} K^{-1})	$\Delta H^{\star b}$ (kJ mol^{-1})	$\Delta G^{\star b}$ (kJ mol^{-1})
Stage 1 (278.17 °C–372.24 °C)	36.1487	0.2299	−52.6447	30.9965	63.6205
Stage 2 (372.24 °C–495.30 °C)	54.5686	9.8897	−22.2852	48.8160	64.2355
Stage 3 (495.30 °C–674.77 °C)	68.6812	37.2202	−12.9203	61.6608	72.5707

[a] Obtained from the slope and intercept of the equation $\log\left[\frac{-\log\log(1-\alpha)}{T^2}\right]$ and $1/T$ (Fig. 3B). [b] Calculated according to eqn (3)–(5).

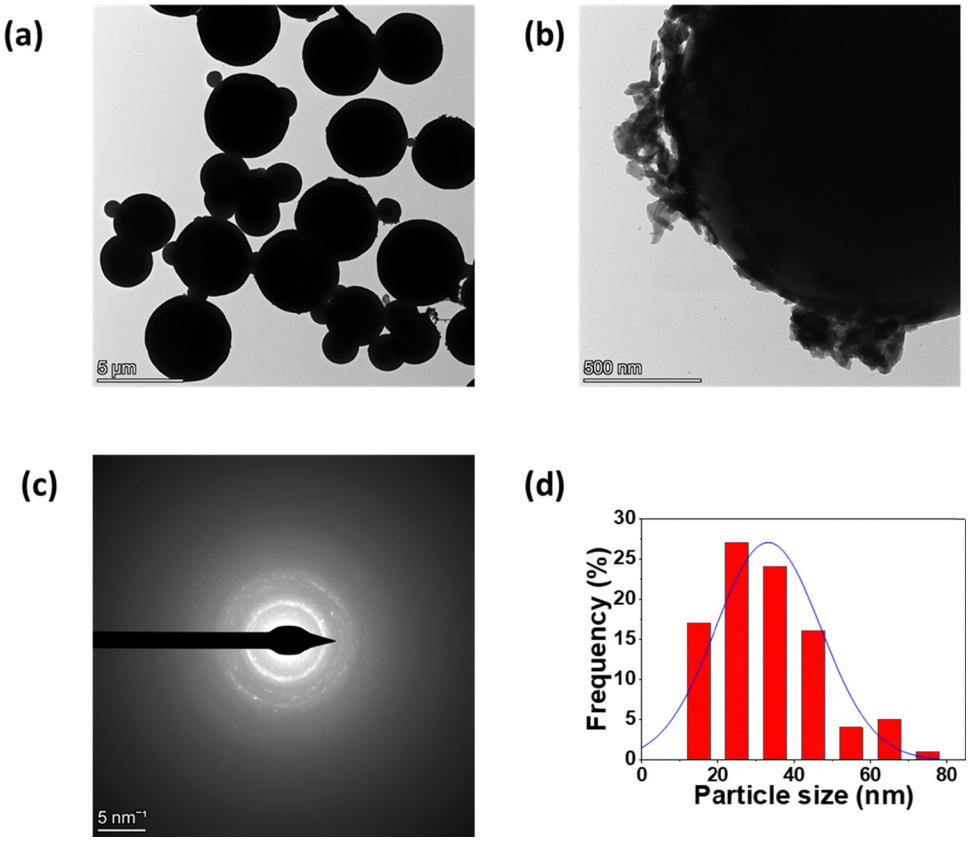

Fig. 4 TEM images (a) and (b); electron beam diffraction (c); and particle size distribution of CuO NPs (d) for CuO/poly(DVB).

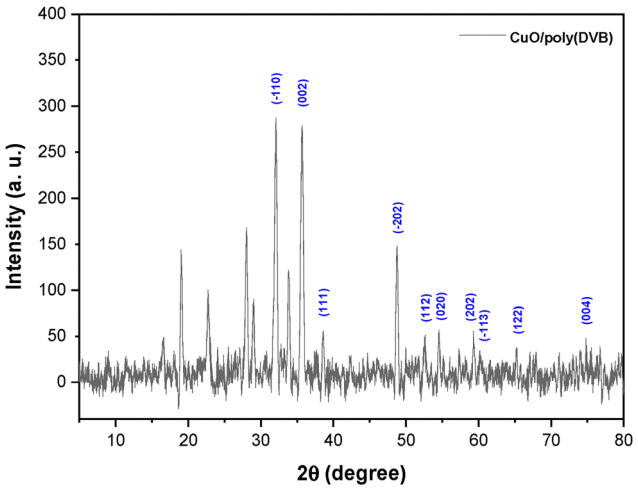

Fig. 5 XRD analysis of CuO/poly(DVB).

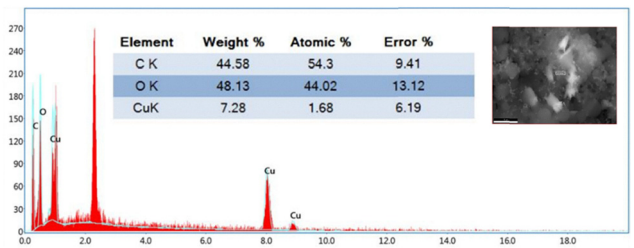

Fig. 6 Energy dispersive X-ray spectroscopy (EDS) of CuO/poly(DVB).

3.6. Brunauer–Emmett–Teller (BET) analysis

The Brunauer–Emmett–Teller (BET) method was utilized to determine the specific surface area and pore volume of the CuO/poly(DVB) catalyst through N_2 adsorption–desorption measurements conducted at 77 K. As illustrated in Fig. 7, the adsorption–desorption isotherm exhibits a type IV BET classification. The composite displayed a specific surface area of 90.0928 $m^2\ g^{-1}$. Barrett–Joyner–Halenda (BJH) analysis further yielded a pore volume of 0.12818 $cm^3\ g^{-1}$ and an average pore radius of 1.682 nm. Based on IUPAC guidelines,[91] which classify porous materials as macroporous (>50 nm), mesoporous (2–50 nm), and microporous (<2 nm) based on pore size, the composite is categorized as a microporous catalyst.

3.7. Catalytic reduction of 4-nitrophenol

3.7.1. Experimental investigation. The catalytic hydrogenation of 4-nitrophenol to 4-aminophenol, mediated by CuO/poly(DVB) in the presence of $NaBH_4$, demonstrates exceptional efficiency, as demonstrated by UV-visible spectrophotometry.[92] Initially, attempts to reduce 4-nitrophenol with only $NaBH_4$ showed no significant change; the yellow color associated with

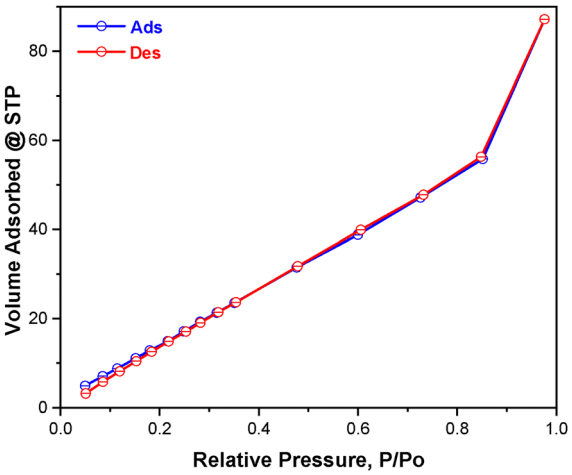

Fig. 7 N_2 adsorption/desorption isotherm of CuO/poly(DVB).

4-nitrophenolate ions persisted, and the absorbance peak at 400 nm showed no significant variation. This indicates that the reaction does not occur in the absence of a catalyst. However, upon introducing the CuO/poly(DVB) catalyst, a rapid transformation was observed. Within just six minutes, the reaction mixture transitioned from yellow to colorless, reflecting the successful conversion to 4-aminophenol. The UV–vis spectra, illustrated in Fig. 8A, support this observation: the absorbance intensity at 400 nm, corresponding to 4-nitrophenol, diminishes over time, while a new peak emerges at 300 nm, confirming the formation of 4-aminophenol. This evidence emphasizes the critical role of the CuO/poly(DVB) catalyst in effectively facilitating the reduction process.

Our investigation was further extended to explore the progression of the catalytic hydrogenation reaction, which was tracked by monitoring the absorbance of 4-nitrophenol at 400 nm at regular two-minute intervals.[67,92,93] During the kinetic studies, the concentration of $NaBH_4$ was maintained at a higher concentration than that of 4-nitrophenol, ensuring that $NaBH_4$ remained effectively constant throughout the reaction. This excess concentration allows us to treat $NaBH_4$ as a constant, thereby making the reaction rate independent of its concentration. Under these conditions, a pseudo-first-order kinetic model can be employed to determine the kinetic parameters. The mathematical representation of the pseudo-first-order reaction is given by:

$$\ln\left(\frac{C_t}{C_0}\right) = -kt \quad (7)$$

where C_0 and C_t represent the initial concentration and concentration at time t of 4-nitrophenol, respectively, while k denotes the observed rate constant. Fig. 8B illustrates the $\ln(A_t/A_0)$ *versus* time plot for the catalytic hydrogenation of 4-nitrophenol mediated by CuO/poly(DVB) under conditions of 0.5 mM $NaBH_4$ and 0.1 mM 4-nitrophenol. The kinetic profile exhibits two distinct phases. During the initial phase (first 2 minutes), $\ln(A_t/A_0)$ remains constant, signifying no observable catalytic activity. This induction period, a well-documented phenomenon,[92,94,95] may arise from factors such as surface oxide layers on CuO nanoparticles, reactant diffusion into the polymer matrix, or interactions between $NaBH_4$ and dissolved oxygen. During this activation stage, catalyst preconditioning occurs without measurable substrate conversion, maintaining a constant $\ln(A_t/A_0)$. Subsequent to the delay phase, $\ln(A_t/A_0)$ decreases linearly with time, corresponding to depletion of 4-nitrophenol through reduction to 4-aminophenol. This transition signifies the onset of effective catalytic behavior in CuO/poly(DVB), enabling efficient transformation of the substrate. The linear correlation adheres to pseudo-first-order kinetics, facilitating the determination of kinetic parameters. The rate constant (k), derived from the slope in Fig. 8B, was calculated as 0.45 ± 0.06 min^{-1}. The corresponding half-life ($t_{1/2}$), calculated using k, was determined to be 1.45 ± 0.19 minutes.

3.7.2. Theoretical investigation. As described in the computational methodology, seven intermediates were identified during the hydrogenation of 4-nitrophenol, aligned with the five principal mechanistic steps depicted in Fig. 9. The reactive

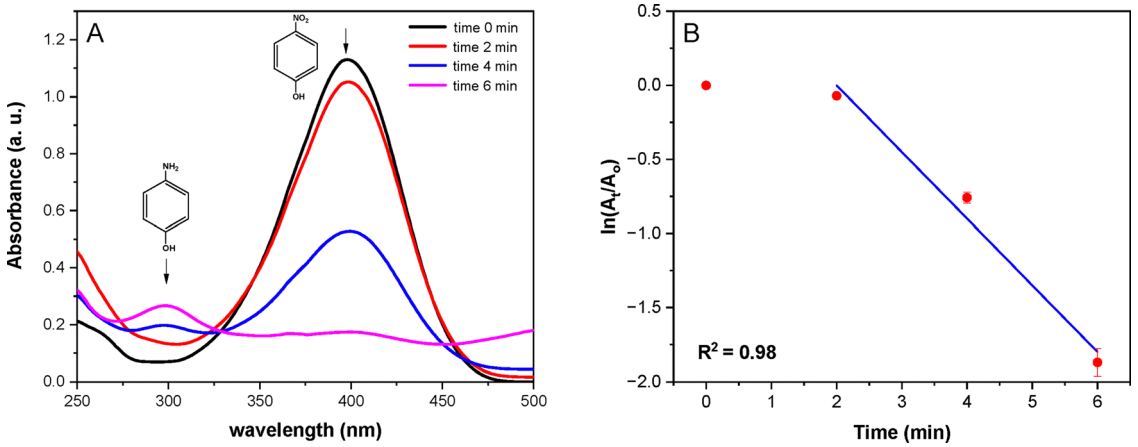

Fig. 8 (A) UV-vis absorption spectra and (B) pseudo-first-order kinetic profile for the catalytic hydrogenation of 4-nitrophenol (4-NP) to 4-aminophenol (4-AP) mediated by $NaBH_4$ as the reducing agent and CuO/poly(DVB) as the catalyst. Experimental conditions: 0.1 mM 4-NP, 0.5 mM $NaBH_4$, and 20 mg CuO/poly(DVB).

complex (RC) comprising 4-nitrophenol adsorbed on the Cu_6O_3 cluster features an interaction between a nitro group oxygen atom and a Cu site, with a Cu–O bond length of 1.96 Å. The initial stage involves proton transfer to the coordinated oxygen atom, yielding the first intermediate complex (IC1). This step shortens the Cu–O bond to 1.90 Å. Subsequent proton transfer to the oxygen atom in IC1 triggers the release of a water molecule and generates the second intermediate complex (IC2), where the organic moiety remains anchored to the Cu_6O_3 cluster *via* the second oxygen atom of the nitro group (Cu–O distance: 1.98 Å). The next step involves a similar protonation process, where the second oxygen is protonated, resulting in a slight elongation of the Cu–O bond distance to 1.99 Å in IC3. This is followed by the elimination of the second water molecule and the formation of IC4. In IC4, the nitrogen atom forms a stronger bond with the copper atom, with a Cu–N bond distance of 1.72 Å. At this stage, the nitrogen carries a charge of −2, requiring two protons to neutralize. Upon protonation, the reduced aromatic compound (IC5) forms, with the protonated nitrogen coordinated to the CuO cluster, exhibiting a Cu–N bond distance of 1.89 Å. In the final product complex (PC), where the nitrogen is fully protonated, the Cu–N bond is weakened, indicating the tendency of the reduced molecule to detach from the metal surface and move into solution. Alternatively, in IC3, a different pathway was identified where the nitrogen is protonated before the elimination of the second oxygen as a water molecule, as depicted in Fig. 9. In this alternative intermediate (IC4*), the Cu–O bond distance was measured at 2.18 Å, indicating a weaker interaction compared to the previous step in IC3. This weakening of the Cu–O bond suggests a higher likelihood of the OH group being released as a water molecule in the subsequent step.

To better understand the role of our catalyst in promoting the reduction mechanism, it is essential to underlne key chemical interactions that take place between different states of nitrophenol and the CuO NP cluster. The proposed reduction mechanism has been thoroughly examined based upon the structural and electronic characterization of the reaction intermediates, which clearly underscore the reduction mechanism. Overall, the experimental findings have been complemented by the DFT calculations, affording fresh atomistic details in identifying the geometries of the possible intermediates. This current level of background understanding is paramount in improving our knowledge to design more potent catalysts for similar processes.

To further improve our knowledge regarding the nature of the chemical interaction involved between nitrophenol and CuO NPs, we display both HOMO and LUMO over RC, IC3 and PC3 intermediates in Fig. 10. Generally, the HOMO is found to be distributed over the aromatic nitro compound molecule, including the atoms involved in ligation to the CuO NPs throughout all the characterized complexes. Conversely, the LUMO is mainly delocalized over CuO metal composites, as observed in all the selected intermediates. Accordingly, our mechanistic findings suggest that the reduction pathway is catalyzed by CuO loaded on the polymer. For both RC and IC6, nitrophenol, an electron-rich molecule, acts as an electron donor, while the metal cluster behaves as an electron acceptor, indicating its electron deficiency. In the case of IC4, the CuO nanocluster is found to be involved in back donation, as noted in its HOMO, while the reduced version of the nitrophenol accepts electrons according to the displayed LUMO. These valuable insights further explain the nature of the interaction between nitrophenol and the CuO NPs, which should deepen our understanding of the actual role played by our catalyst in facilitating the reduction reaction. We propose that the greater the propensity of the metal catalyst to act as an electron acceptor, the more efficient it is in facilitating the reduction reaction of nitrophenol-containing compounds.

3.8. Catalyst reusability

Following the catalytic hydrogenation of 4-nitrophenol to 4-aminophenol, the CuO/poly(DVB) catalyst was recovered *via* centrifugation, rinsed with methanol, dried, and directly reused in successive cycles. Reusability tests (Fig. 11) revealed that the composite retained significant catalytic efficiency over four cycles, with conversion rates declining from 84.6% (cycle 1) to 79%, 78.23%, and 78% in subsequent cycles. Despite this modest decline, the catalyst maintained robust activity, demonstrating structural integrity and stability under the reaction conditions. These findings underscore the reusability of CuO/poly(DVB) successive catalytic cycles.

To evaluate the structural stability of the CuO/poly(DVB) catalyst after multiple reuse cycles, FTIR and XRD analyses were performed on the recovered catalyst following four consecutive reductions of 4-nitrophenol. As shown in Fig. 12A, the FTIR spectra of the fresh and reused catalysts exhibit no significant differences. The characteristic Cu–O stretching band around 619 cm^{-1} and the aromatic C=C stretching vibrations between 1447 and 1697 cm^{-1} remain present, indicating the preservation of both the copper oxide phase

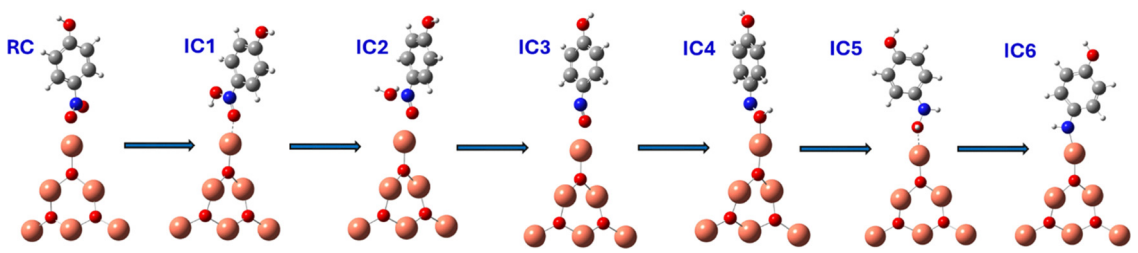

Fig. 9 Reaction pathway for the hydrogenation of nitrophenol to aminophenol catalyzed by CuO nanoparticles, as investigated through density functional theory (DFT) calculations.

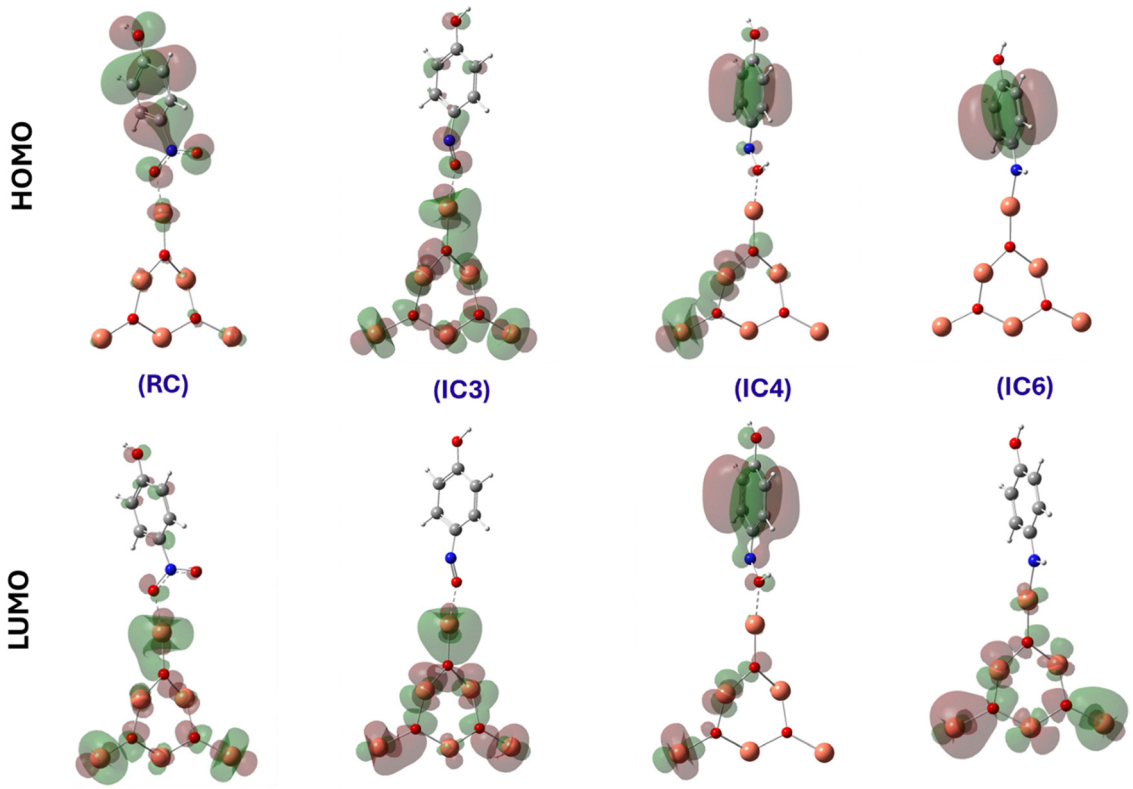

Fig. 10 The HOMO (top) and LUMO (bottom) Frontier orbitals displayed over three key intermediates determined throughout the reduction mechanism.

and the polymer backbone. This suggests that the CuO nanoparticles remained anchored to the polymer matrix without chemical degradation during the catalytic cycles. Similarly, the XRD patterns in Fig. 12B reveal that the reused catalyst retains the main diffraction peaks associated with monoclinic CuO, as seen in the fresh catalyst. No additional peaks corresponding to byproducts, metallic copper, or copper hydroxide phases were observed, and no notable broadening or shifting of peaks occurred. This confirms the crystallographic stability of the CuO nanoparticles during repeated use. The retention of peak intensity also supports the notion that the catalyst did not undergo significant particle agglomeration or phase transformation. Together, these post-reaction characterizations strongly support the excellent chemical and structural stability of the CuO/poly(DVB) catalyst.

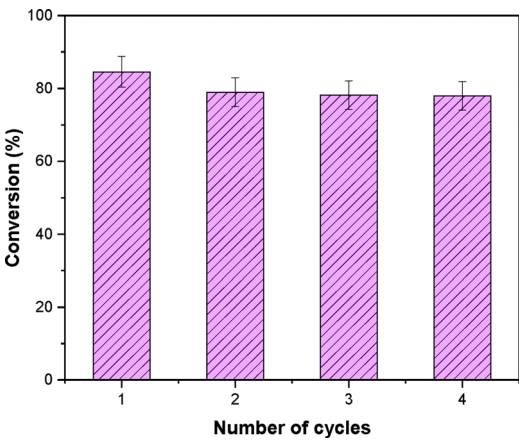

Fig. 11 Recycling experiments for the catalytic reduction of 4-NP to 4-AP. Reaction conditions: [4-NP] = 0.1 mM, [$NaBH_4$] = 10 mM, weight of CuO/poly(DVB) is 20 mg.

To evaluate the catalytic performance of the CuO/DVB catalyst, its efficiency in the hydrogenation of 4-nitrophenol (4-NP) was benchmarked against other catalysts documented in the literature. The comparative results are presented in Table 2. Although a direct comparison is complicated by differences in experimental parameters, such as varying 4-NP and $NaBH_4$ concentrations and catalyst dosage, the CuO/DVB stands out as one of the most effective catalysts. It offers notable advantages over similar catalysts, particularly in terms of ease of preparation and catalytic effectiveness.

4. Conclusion

In this study, CuO/poly(DVB) was demonstrated to be a highly effective heterogeneous catalyst for the reduction of toxic nitrophenol. The poly(DVB) matrix serves as an optimal support for CuO nanoparticles, enabling their uniform dispersion as nanoclusters with an average crystallite size of 33 nm. The catalytic hydrogenation of nitrophenol was achieved within 6 min, exhibiting a rate constant of 0.45 min^{-1} and a half-life of 1.45 min. Thermogravimetric analysis confirmed the thermal stability of the composite up to 278.17 °C. Notably, the catalyst

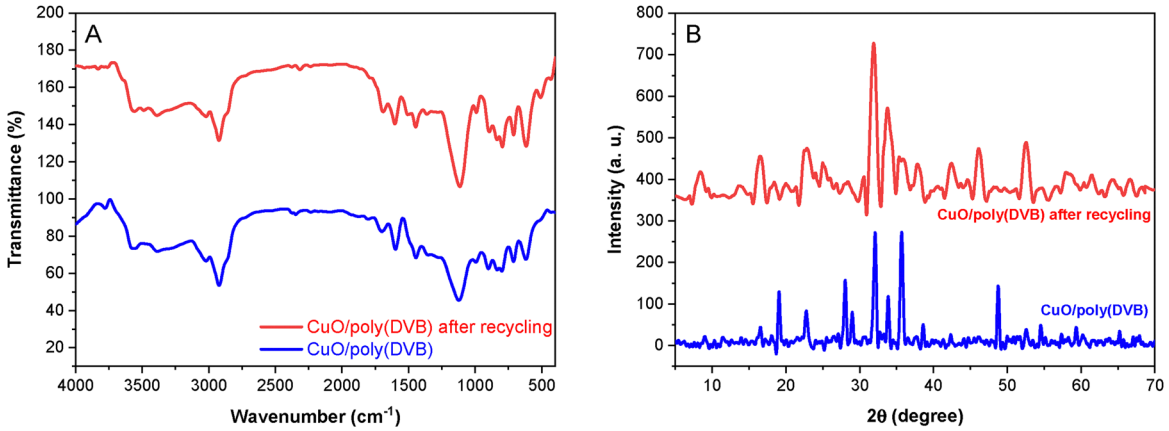

Fig. 12 (A) FTIR spectra and (B) XRD patterns of the CuO/poly(DVB) catalyst before and after four catalytic recycling cycles.

Table 2 Comparative analysis of catalytic hydrogenation of 4-nitrophenol (4-NP) using various catalysts

		Reaction conditions					
No.	Catalyst	[4-NP] ($\times 10^{-3}$ mmol)	[$NaBH_4$] ($\times 10^{-3}$ mmol)	Wt. cat. (mg)	Time (min)	K (min^{-1})	Ref.
1	CuO nanoleaves	0.36	30.00	1.00	15.00	0.02	96
2	CuO flowers	0.25	50.00	2.00	4.00	0.56	97
3	Pd/CuO NPs	62.50	6250.00	7.00	1.00	3.30	98
4	CuO@C composite	100.00	2250.00	50.00	18.00	0.36	99
5	CuO/ZnO/eggshell	2.00	1320.00	20.00	30.00	0.20	100
6	CuO/Cu_2O nanowires	0.25	50.00	0.10	4.00	0.50	101
7	CuO NPs	14.38	528.00	5.00	12.00	0.38	102
8	CuO/poly(DVB)	5.00	500.00	20.00	6.00	0.45	Present study

exhibited excellent recyclability, retaining significant activity over four consecutive cycles after facile separation from the reaction mixture. Complementary DFT simulations further elucidated the mechanistic pathway, reinforcing the utility of the composite in sustainable catalysis. In addition, CuO/poly(DVB) is found to be a competitive catalyst with superior advantages over similar catalysts. Specifically, in addition to providing similar activities, it has shown a tendency to be more readily prepared. Our knowledge of the reduction mechanism has been further enriched by obtaining atomistic details of the reaction pathway through powerful DFT calculations. Implementing a chemical model containing hazardous nitrophenol loaded over CuO NPs, all the intermediates throughout the catalytic reduction have been completely identified. Analysis of the HOMO and LUMO frontier orbitals further corroborates our results by highlighting the significant electronic interactions between the intermediates of the aromatic compound and the CuO NPs. This catalyst should afford an alternative, sustainable catalytic approach for removing the toxic organic pollutants present in industrial wastewater. We propose that the structural findings obtained from our study could also be applied to the reduction of similar nitrophenol compounds.

Author contributions

E. E.: conceptualization, methodology, validation, formal analysis, investigation, resources, data curation, writing – review & editing. E. I.: computational analysis, investigation, visualization, writing – original draft. Tamaki Nakano: conceptualization, writing – review & editing. A. E. project administration, investigation, resources, formal analysis. M. A: project administration, computational analysis, investigation, visualization, data analysis, resources, writing – review & editing.

Conflicts of interest

We declare that we have no known competing financial interests or personal relationships that could have appeared to influence the work reported in this paper.

Data availability

The data that support the findings of this study are available from the corresponding author upon reasonable request.

Acknowledgements

This research was supported in part by Joint Usage/Research program Institute for Catalysis, Hokkaido University, Japan Grant number ID 21B1010. The authors acknowledge the Central Laboratory at the Faculty of Science, Damietta University, for providing access to UV-vis and FTIR spectroscopy facilities.

References

1 A. Serrà, R. Artal, M. Pozo, J. Garcia-Amorós and E. Gómez, Simple Environmentally-Friendly Reduction of 4-Nitrophenol, *Catalysts*, 2020, **10**(4), 458.
2 E. M. Sitinjak, I. Masmur, N. V. M. D. Marbun, P. E. Hutajulu, G. Gultom and Y. Sitanggang, Direct Z-scheme of n-type CuS/p-type ZnS@electrospun PVP nanofiber for the highly efficient catalytic reduction of 4-nitrophenol and mixed dyes, *RSC Adv.*, 2022, **12**(25), 16165–16173.
3 G. Zhu, Q. Tang, M. Huang, J. Yang, R. Xu and J. Liu, Polyaniline nanoconical array on carbon nanofiber for supersensitive determination of nitrophenol, *Sens. Actuators, B*, 2020, **320**, 128593.
4 E. Elbayoumy, M. O. Elassi, G. M. Khairy, E. A. Moawed and M. M. aboelnga, Development of efficient fluorescent sensor for the detection of hazard aromatic nitro compounds via N-(1-naphthyl)ethylenediamine: Experimental and DFT studies, *J. Mol. Liq.*, 2023, **391**, 123270.
5 B. Liang, H. Cheng, J. D. Van Nostrand, J. Ma, H. Yu and D. Kong, *et al.*, Microbial community structure and function of Nitrobenzene reduction biocathode in response to carbon source switchover, *Water Res.*, 2014, **54**, 137–148.
6 M. Kulkarni and A. Chaudhari, Kinetic studies on mineralization of p-nitrophenol by Pseudomonas putida at low and high concentration, *Indian J. Chem. Technol.*, 2006, **13**(1), 60–64.
7 H. Ali and A. M. Ismail, Recyclable and Biodegradable Ag@Chitosan Nanocomposite Beads Synthesized in One-step for Catalytic Hydrogenation of 4-Nitrophenol, *J. Polym. Environ.*, 2022, **30**(8), 3379–3390.
8 M. I. Din, R. Khalid, Z. Hussain, T. Hussain, A. Mujahid and J. Najeeb, *et al.*, Nanocatalytic Assemblies for Catalytic Reduction of Nitrophenols: A Critical Review, *Crit. Rev. Anal. Chem.*, 2020, **50**(4), 322–338.
9 T. Rasheed, F. Nabeel, K. Rizwan, M. Bilal, T. Hussain and S. A. Shehzad, Conjugated supramolecular architectures as state-of-the-art materials in detection and remedial measures of nitro based compounds: A review, *TrAC, Trends Anal. Chem.*, 2020, **129**, 115958.
10 T. Rasheed, C. Li, F. Nabeel, W. Huang and Y. Zhou, Self-assembly of alternating copolymer vesicles for the highly selective, sensitive and visual detection and quantification of aqueous Hg2+, *Chem. Eng. J.*, 2019, **358**, 101–109.
11 T. Rasheed, C. Li, L. Fu, F. Nabeel, C. Yu and L. Gong, *et al.*, Development and characterization of newly engineered chemosensor with intracellular monitoring potentialities and lowest detection of toxic elements, *J. Mol. Liq.*, 2018, **272**, 440–449.
12 T. Rasheed, C. Li, M. Bilal, C. Yu and H. M. N. Iqbal, Potentially toxic elements and environmentally-related pollutants recognition using colorimetric and ratiometric fluorescent probes, *Sci. Total Environ.*, 2018, **640–641**, 174–193.
13 T. Rasheed, C. Li, Y. Zhang, F. Nabeel, J. Peng and J. Qi, *et al.*, Rhodamine-based multianalyte colorimetric probe with potentialities as on-site assay kit and in biological systems, *Sens. Actuators, B*, 2018, **258**, 115–124.
14 F. Nabeel and T. Rasheed, Rhodol-conjugated polymersome sensor for visual and highly-sensitive detection of hydrazine in aqueous media, *J. Hazard. Mater.*, 2020, **388**, 121757.
15 T. Rasheed, C. Li, F. Nabeel, M. Qi, Y. Zhang and C. Yu, Real-time probing of mercury using an efficient ''turn-on'' strategy with potential as in-field mapping kit and in live cell imaging, *New J. Chem.*, 2018, **42**(13), 10940–10946.
16 M. M. Ayad, W. A. Amer and M. G. Kotp, Magnetic polyaniline-chitosan nanocomposite decorated with palladium nanoparticles for enhanced catalytic reduction of 4-nitrophenol, *Mol. Catal.*, 2017, **439**, 72–80.
17 A. I. Raafat, G. A. Mahmoud and T. B. Mostafa, Efficient Catalytic Reduction of Hazardous Anthropogenic Pollutant, 4-Nitrophenol Using Radiation Synthesized (Polyvinyl Pyrrolidone/Acrylic Acid)-Silver Nanocomposite Hydrogels, *J. Inorg. Organomet. Polym. Mater.*, 2020, **30**(8), 3116–3125.
18 N. Anusuya, C. Pragathiswaran and G. Thulasi, Catalytic reduction of 4-nitrophenol to 4- amino phenol by chitosan/TiO_2–Fe_2O_3 nanomaterial, *Mater. Today Proc.*, 2021, **37**, 3759–3763.
19 J. Sun, Y. Fu, G. He, X. Sun and X. Wang, Catalytic hydrogenation of nitrophenols and nitrotoluenes over a palladium/graphene nanocomposite, *Catal. Sci. Technol.*, 2014, **4**(6), 1742–1748.
20 X. Ren, L. Tang, J. Wang, E. Almatrafi, H. Feng and X. Tang, *et al.*, Highly efficient catalytic hydrogenation of nitrophenols by sewage sludge derived biochar, *Water Res.*, 2021, **201**, 117360.
21 K. Urkude, S. R. Thakare and S. Gawande, An energy efficient photocatalytic reduction of 4-nitrophenol, *J. Environ. Chem. Eng.*, 2014, **2**(1), 759–764.
22 T. Sismanoglu and S. Pura, Adsorption of aqueous nitrophenols on clinoptilolite, *Colloids Surf., A*, 2001, **180**(1–2), 1–6.
23 S. M. Tabatabaei, S. Dastmalchi, A. Mehrizad and P. Gharbani, Enhancement of 4-Nitrophenol ozonation in water bynano zno catalyst, *Iran. J. Environ. Health Sci. Eng.*, 2011, **8**(4), 363–372.
24 M. Kulkarni and A. Chaudhari, Biodegradation of p-nitrophenol by P. putida, *Bioresour. Technol.*, 2006, **97**(8), 982–988.
25 F. Xie, Y. Xu, K. Xia, C. Jia and P. Zhang, Alternate pulses of ultrasound and electricity enhanced electrochemical process for p-nitrophenol degradation, *Ultrason. Sonochem.*, 2016, **28**, 199–206.
26 F. U. Khan, Asimullah, S. B. Khan, T. Kamal, A. M. Asiri and I. U. Khan, *et al.*, Novel combination of zero-valent Cu and Ag nanoparticles@cellulose acetate nanocomposite for the reduction of 4-nitro phenol, *Int. J. Biol. Macromol.*, 2017, **102**, 868–877.
27 G. Tokazhanov, S. Han and W. Lee, Enhanced catalytic reduction of p-nitrophenol by nano zerovalent iron - supported metal catalysts, *Catal. Commun.*, 2021, **158**, 106337.

28 E. Da'na, A. Taha and M. R. El-Aassar, Catalytic Reduction of p-Nitrophenol on MnO2/Zeolite -13X Prepared with Lawsonia inermis Extract as a Stabilizing and Capping Agent, *Nanomaterials*, 2023, **13**(4), 785.

29 E. Elbayoumy, A. A. El-Bindary, T. Nakano and M. M. Aboelnga, Silver nanoparticles immobilized on crosslinked vinyl polymer for catalytic reduction of nitrophenol: experimental and computational studies, *Sci. Rep.*, 2025, **15**(1), 717.

30 A. Mondal, A. Mondal, B. Adhikary and D. K. Mukherjee, Cobalt nanoparticles as reusable catalysts for reduction of 4-nitrophenol under mild conditions, *Bull. Mater. Sci.*, 2017, **40**(2), 321–328.

31 E. Elbayoumy, Y. Wang, J. Rahman, C. Trombini, M. Bando and Z. Song, *et al.*, Pd Nanoparticles-Loaded Vinyl Polymer Gels: Preparation, Structure and Catalysis, *Catalysts*, 2021, **11**(1), 137.

32 M. Ghorbanloo and H. Nosrati Fallah, Silver nanoparticle embedded anionic crosslinked copolymer hydrogels: an efficient catalyst, *J. Porous Mater.*, 2020, **27**(3), 765–777.

33 Z. H. Farooqi, S. R. Khan, T. Hussain, R. Begum, K. Ejaz and S. Majeed, *et al.*, Effect of crosslinker feed content on catalaytic activity of silver nanoparticles fabricated in multiresponsive microgels, *Korean J. Chem. Eng.*, 2014, **31**(9), 1674–1680.

34 R. R. Palem, S. D. Ganesh, N. Saha, J. Kronek and P. Sáha, 'Green' synthesis of silver polymer Nanocomposites of poly (2-isopropenyl-2- oxazoline-*co*-*N*-vinylpyrrolidone) and its catalytic activity, *J. Polym. Res.*, 2018, **25**(7), 152.

35 S. Varshney, R. Bar-Ziv and T. Zidki, On the Remarkable Performance of Silver-based Alloy Nanoparticles in 4-Nitrophenol Catalytic Reduction, *ChemCatChem*, 2020, **12**(18), 4680–4688.

36 S. R. Khan, Z. H. Farooqi, M. Ajmal, M. Siddiq and A. Khan, Synthesis, Characterization, and Silver Nanoparticles Fabrication in N-isopropylacrylamide-Based Polymer Microgels for Rapid Degradation of p-Nitrophenol, *J. Dispers. Sci. Technol.*, 2013, **34**(10), 1324–1333.

37 Y. Lu, Y. Shi, Y. Wang, J. Cao, J. Wang and Y. Zheng, *et al.*, A defect-enriched PdMo bimetallene for ethanol oxidation reaction and 4-nitrophenol reduction, *Chem. Commun.*, 2024, **60**(24), 3323–3326.

38 F. Wei, M. Luo, J. Lan, F. Xie, L. Cai and T. S. Chan, *et al.*, Pd Atomic Engineering of Nanoporous Ni/NiO for Efficient Nitrophenol Hydrogenation Reaction, *ACS Appl. Mater. Interfaces*, 2023, **15**(22), 26746–26754.

39 Y. Wang, Y. Lu, Y. Shi, J. Wang, Y. Zheng and J. Pan, *et al.*, Realizing highly-efficient urea oxidation via decreasing the energy barrier of deprotonation over regulated electronic structure of Co doped Ni(OH)2, *Appl. Surf. Sci.*, 2023, **640**, 158391.

40 L. Que, L. Lu, Y. Xu, X. Xu, M. Zhu and J. Pan, *et al.*, The Ni^{2+}–$LaNiO_3$/CdS hollow core–shell heterojunction towards enhanced visible light overall water splitting H2 evolution via HER/OER synergism of Ni^{2+}/Ov, *Chem. Eng. J.*, 2023, **469**, 143902.

41 P. Jing, C. He, S. Huang, H. Li, J. Liu and Y. Cui, *et al.*, 2D Z-scheme heterojunction and oxygen deficiency synergistically boosting the photocatalytic activity of a layered $BaTiO_3$/$BiOIO_3$ composite, *Appl. Mater. Today*, 2022, **29**, 101574.

42 P. Zhang, Y. Shi, Y. Zhang, S. Feng, L. Shi and J. Pan, *et al.*, Self-cleaning transparent pn junction in $CuAlO_2$/WO_3 via high entropy perovskite oxide $La(Cu_{0.2}Cr_{0.2}Ni_{0.2}Fe_{0.2}Co_{0.2})O_3$ transition layer for enhanced photovoltaic conversion, *Chem. Eng. J.*, 2024, **487**, 150727.

43 S. Shen, H. Zhang, K. Song, Z. Wang, T. Shang and A. Gao, *et al.*, Multi-d Electron Synergy in $LaNi_{1-x}Co_xRu$ Intermetallics Boosts Electrocatalytic Hydrogen Evolution, *Angew. Chem., Int. Ed.*, 2024, **63**(1), e202315340.

44 P. Mondal, A. Sinha, N. Salam, A. S. Roy, N. R. Jana and S. M. Islam, Enhanced catalytic performance by copper nanoparticle-graphene based composite, *RSC Adv.*, 2013, **3**(16), 5615–5623.

45 R. García-Álvarez, A. E. Díaz-Álvarez, P. Crochet and V. Cadierno, Ruthenium-catalyzed one-pot synthesis of primary amides from aldehydes in water, *RSC Adv.*, 2013, **3**(17), 5889–5894.

46 M. Hu, J. S. Jiang, F. X. Bu, X. L. Cheng, C. C. Lin and Y. Zeng, Hierarchical magnetic iron(III) oxides prepared by solid-state thermal decomposition of coordination polymers, *RSC Adv.*, 2012, **2**(11), 4782–4786.

47 Y. W. C. Cao, R. Jin and C. A. Mirkin, Nanoparticles with Raman spectroscopic fingerprints for DNA and RNA detection, *Science*, 2002, **297**(5586), 1536–1540.

48 Z. Zhang, H. Che, Y. Wang, L. Song, Z. Zhong and F. Su, Preparation of hierarchical dandelion-like CuO microspheres with enhanced catalytic performance for dimethyldichlorosilane synthesis, *Catal. Sci. Technol.*, 2012, **2**(9), 1953–1960.

49 S. M. Salman, S. Narayanaperumal, R. S. Schwab, C. R. Bender, O. E. D. Rodrigues and L. Dornelles, CuO nano particles and [bmim]BF4: An application towards the synthesis of chiral β-seleno amino derivatives via ring opening reaction of aziridines with diorganyl diselenides, *RSC Adv.*, 2012, **2**(22), 8478–8482.

50 S. Liu, J. Tian, L. Wang, Y. Luo and X. Sun, One-pot synthesis of CuO nanoflower-decorated reduced graphene oxide and its application to photocatalytic degradation of dyes, *Catal. Sci. Technol.*, 2012, **2**(2), 339–344.

51 J. Zhu, G. Zeng, F. Nie, X. Xu, S. Chen and Q. Han, *et al.*, Decorating graphene oxide with CuO nanoparticles in a water-isopropanol system, *Nanoscale*, 2010, **2**(6), 988–994.

52 S. Gandhi, R. H. H. Subramani, T. Ramakrishnan, A. Sivabalan, V. Dhanalakshmi and M. R. G. Nair, *et al.*, Ultrasound assisted one pot synthesis of nano-sized CuO and its nanocomposite with poly(vinyl alcohol), *J. Mater. Sci.*, 2010, **45**(6), 1688–1694.

53 X. Yao, F. Gao, Q. Yu, L. Qi, C. Tang and L. Dong, *et al.*, NO reduction by CO over CuO-CeO2 catalysts: Effect of preparation methods, *Catal. Sci. Technol.*, 2013, **3**(5), 1355–1366.

54 Z. Zhang, H. Che, Y. Wang, J. Gao, X. She and J. Sun, *et al.*, Flower-like CuO microspheres with enhanced catalytic performance for dimethyldichlorosilane synthesis, *RSC Adv.*, 2012, **2**(6), 2254–2256.

55 S. Sun, X. Zhang, Y. Sun, J. Zhang, S. Yang and X. Song, *et al.*, A facile strategy for the synthesis of hierarchical CuO nanourchins and their application as non-enzymatic glucose sensors, *RSC Adv.*, 2013, **3**(33), 13712–13719.
56 H. Kang, H. J. Lee, J. C. Park, H. Song and K. H. Park, Solvent-free microwave promoted [3+2] cycloaddition of alkyne-azide in uniform CuO hollow nanospheres, *Top. Catal.*, 2010, 523–528.
57 P. Kaur, J. T. Hupp and S. T. Nguyen, Porous organic polymers in catalysis: Opportunities and challenges, *ACS Catal.*, 2011, **1**, 819–835.
58 G. I. Dzhardimalieva, A. K. Zharmagambetova, S. E. Kudaibergenov and I. E. Uflyand, Polymer-Immobilized Clusters and Metal Nanoparticles in Catalysis, *Kinet. Catal.*, 2020, **61**(2), 198–223.
59 M. Li, X. Ren, Y. Gao, M. Mu, S. Zhu and D. Li, *et al.*, Poly(divinylbenzene) as a fiber coating for headspace solid-phase microextraction of polycyclic aromatic hydrocarbons from river water, *Chem. Commun.*, 2022, **58**(54), 7574–7577.
60 Y. P. Liang, Y. Bin Chan, M. Aminuzzaman, M. Shahinuzzaman, S. Djearamane and K. Thiagarajah, Green Synthesis and Characterization of Copper Oxide Nanoparticles from Durian (Durio zibethinus) Husk for Environmental Applications, *Catalysts*, 2025, **15**(3), 275.
61 Y. B. Chan, M. Aminuzzaman, X. T. Chuah, K. Li, P. Balu and L. S. Wong, Review in green synthesis mechanisms, application, and future prospects for Garcinia mangostana L. (mangosteen)-derived nanoparticles, *Nanotechnol. Rev.*, 2025, **14**(1), 20250157.
62 H. Subramaniam, C. K. Lim, L. H. Tey, L. S. Wong and S. Djearamane, Oxidative stress-induced cytotoxicity of HCC2998 colon carcinoma cells by ZnO nanoparticles synthesized from Calophyllum teysmannii, *Sci. Rep.*, 2024, **14**(1), 30198.
63 C. H. Raksha, M. P. Yogeesh and N. S. Shetty, Recent advances in the synthesis of polymer supported catalysts: a review, *Discover Appl. Sci.*, 2025, **7**(6), 565.
64 N. Silva, S. Ramírez, I. Díaz, A. Garcia and N. Hassan, Easy, quick, and reproducible sonochemical synthesis of CuO nanoparticles, *Materials*, 2019, **12**(5), 804.
65 S. S. Satapathy, P. Bhol, A. Chakkarambath, J. Mohanta, K. Samantaray and S. K. Bhat, *et al.*, Thermo-responsive PNIPAM-metal hybrids: An efficient nanocatalyst for the reduction of 4-nitrophenol, *Appl. Surf. Sci.*, 2017, **420**, 753–763.
66 M. K. Guria, M. Majumdar and M. Bhattacharyya, Green synthesis of protein capped nano-gold particle: An excellent recyclable nano-catalyst for the reduction of nitro-aromatic pollutants at higher concentration, *J. Mol. Liq.*, 2016, **222**, 549–557.
67 R. Begum, K. Naseem, E. Ahmed, A. Sharif and Z. H. Farooqi, Simultaneous catalytic reduction of nitroarenes using silver nanoparticles fabricated in poly(N-isopropylacrylamide-acrylic acid-acrylamide) microgels, *Colloids Surf., A*, 2016, **511**, 17–26.
68 J. P. Perdew, M. Ernzerhof and K. Burke, Rationale for mixing exact exchange with density functional approximations, *J. Chem. Phys.*, 1996, **105**(22), 9982–9985.
69 A. D. Becke, Density-functional thermochemistry. III. The role of exact exchange, *J. Chem. Phys.*, 1993, **98**(7), 5648–5652.
70 P. J. Stephens, F. J. Devlin, C. F. Chabalowski and M. J. Frisch, Ab Initio Calculation of Vibrational Absorption and Circular Dichroism Spectra Using Density Functional Force Fields, *J. Phys. Chem.*, 1994, **98**(45), 11623–11627.
71 M. Abdul Latif, J. W. J. Wu, R. Moriyama, M. Nakano, K. Ohshimo and F. Misaizu, Stable Compositions and Structures of Copper Oxide Cluster Cations Cu nO m+ (n = 2-8) Studied by Ion Mobility Mass Spectrometry, *ACS Omega*, 2018, **3**(12), 18705–18713.
72 M. M. Aboelnga and J. W. Gauld, Comparative QM/MM study on the inhibition mechanism of β-Hydroxynorvaline to Threonyl-tRNA synthetase, *J. Mol. Graphics Modell.*, 2022, **115**, 108224.
73 M. M. Aboelnga, Mechanistic insights into the chemistry of compound I formation in heme peroxidases: quantum chemical investigations of cytochrome *c* peroxidase, *RSC Adv.*, 2022, **12**(24), 15543–15554.
74 S. A. Elsayed, E. E. Saleh, M. M. Aboelnaga and E. A. Toson, Experimental and computational studies of silver(I) dibenzoylmethane-based complexes, interaction with DNA/RNA/BSA biomolecules, and in vitro cytotoxic activity, *J. Inorg. Biochem.*, 2023, **241**, 112132.
75 M. M. Aboelnga and J. W. Gauld, Roles of the Active Site Zn(II) and Residues in Substrate Discrimination by Threonyl-tRNA Synthetase: An MD and QM/MM Investigation, *J. Phys. Chem. B*, 2017, **121**(25), 6163–6174.
76 M. S. Mohy Eldin, Y. A. Aggour, M. R. El-Aassar, G. E. Beghet and R. R. Atta, Development of nano-crosslinked polyacrylonitrile ions exchanger particles for dyes removal, *Desalin. Water Treat.*, 2016, **57**(9), 4255–4266.
77 M. Fathy, T. Abdel Moghny, A. E. Awad Allah and A. E. Alblehy, Cation exchange resin nanocomposites based on multi-walled carbon nanotubes, *Appl. Nanosci.*, 2014, **4**(1), 103–112.
78 M. Sobiesiak, M. Grochowicz and J. O. Tomasik, Sorption properties of polydivinylbenzene polymers towards phenolic compounds and pharmaceuticals, *Colloids Interfaces*, 2019, **3**(1), 19.
79 A. Varughese, R. Kaur and P. Singh Green Synthesis and Characterization of Copper Oxide Nanoparticles Using Psidium guajava Leaf Extract. In: IOP Conference Series: Materials Science and Engineering. 2020.
80 M. A. Diab, N. A. El-Ghamaz, F. S. Mohamed and E. M. El-Bayoumy, Conducting polymers VIII: Optical and electrical conductivity of poly(bis-m-phenylenediaminosulphoxide), *Polym. Test.*, 2017, **63**, 440–447.
81 E. Elbayoumy, N. A. El-Ghamaz, F. S. Mohamed, M. A. Diab and T. Nakano, Dielectric permittivity, AC electrical conductivity and conduction mechanism of high crosslinked-vinyl polymers and their Pd(OAc)2 composites, *Polymers*, 2021, **13**(17), 3005.
82 Y. A. Aggour, E. R. Kenawy, M. Magdy and E. Elbayoumy, Establishing a productive heterogeneous catalyst based on

silver nanoparticles supported on a crosslinked vinyl polymer for the reduction of nitrophenol, *RSC Adv.*, 2024, **14**(41), 30127–30139.

83 V. Indira and G. Parameswaran, Thermal decomposition kinetics of salicylideneaminofluorene complexes of cobalt(II) and nickel(II), *Thermochim. Acta*, 1986, **101**(C), 145–154.

84 L. Zhou, Y. Wang, Q. Huang and J. Cai, Thermogravimetric characteristics and kinetic of plastic and biomass blends co-pyrolysis, *Fuel Process. Technol.*, 2006, **87**(11), 963–999.

85 N. A. El-Ghamaz, T. S. Ahmed and D. A. Salama, Optical, dielectrical properties and conduction mechanism of copolymer (*N*,*N*′-bissulphinyl-*m*-benzenediamine-*p*-phenylenediamine), *Eur. Polym. J.*, 2017, **93**, 8–20.

86 E. Elbayoumy, M. Elhendawy, M. M. Gaafar, E. Moawed and M. M. aboelnga, Novel fluorescent sensor based on triazole-pyridine derivative for selective detection of mercury (II) ions in different real water samples: Experimental and DFT calculations, *J. Mol. Liq.*, 2024, **401**, 124589.

87 S. K. Akay, A. Peksoz and A. Kara, Magnetic responses of divinylbenzene-Fe3O4 composite film deposited by free radical polymerization method, *J. Supercond. Novel Magn.*, 2018, **31**(3), 849–854.

88 D. Li, F. Wang, X. Zhang, L. Liang and J. Sun, The efficient removal of organic pollutant over magnetic mesoporous polymer, *J. Porous Mater.*, 2014, **21**(5), 811–817.

89 Y. J. Lee and Y. Park, Graphene oxide grafted gold nanoparticles and silver/silver chloride nanoparticles green-synthesized by a Portulaca oleracea extract: Assessment of catalytic activity, *Colloids Surf., A*, 2020, **607**, 125527.

90 Z. H. Farooqi, K. Naseem, R. Begum and A. Ijaz, Catalytic Reduction of 2-Nitroaniline in Aqueous Medium Using Silver Nanoparticles Functionalized Polymer Microgels, *J. Inorg. Organomet. Polym. Mater.*, 2015, **25**(6), 1554–1568.

91 B. D. Zdravkov, J. J. Čermák, M. Šefara and J. Janků, Pore classification in the characterization of porous materials: A perspective, *Cent. Eur. J. Chem.*, 2007, **5**(2), 385–395.

92 R. Begum, Z. H. Farooqi, E. Ahmed, K. Naseem, S. Ashraf and A. Sharif, *et al.*, Catalytic reduction of 4-nitrophenol using silver nanoparticles-engineered poly(N-isopropylacrylamide-*co*-acrylamide) hybrid microgels, *Appl. Organomet. Chem.*, 2017, **31**(2), e3563.

93 D. Yang, M. Viitasuo, F. Pooch, H. Tenhu and S. Hietala, Poly(*N*-acryloylglycinamide) microgels as nanocatalyst platform, *Polym. Chem.*, 2018, **9**(4), 517–524.

94 M. Ajmal, Z. H. Farooqi and M. Siddiq, Silver nanoparticles containing hybrid polymer microgels with tunable surface plasmon resonance and catalytic activity, *Korean J. Chem. Eng.*, 2013, **30**(11), 2030–2036.

95 Y. Y. Liu, X. Y. Liu, J. M. Yang, D. L. Lin, X. Chen and L. S. Zha, Investigation of Ag nanoparticles loading temperature responsive hybrid microgels and their temperature controlled catalytic activity, *Colloids Surf., A*, 2012, **393**, 105–110.

96 A. Bhattacharjee and M. Ahmaruzzaman, Green synthesis of 2D CuO nanoleaves (NLs) and its application for the reduction of p-nitrophenol, *Mater. Lett.*, 2015, **161**, 79–82.

97 K. Sahu, R. Singhal and S. Mohapatra, Morphology Controlled CuO Nanostructures for Efficient Catalytic Reduction of 4-Nitrophenol, *Catal. Lett.*, 2020, **150**(2), 471–481.

98 M. Nasrollahzadeh, S. M. Sajadi, A. Rostami-Vartooni and M. Bagherzadeh, Green synthesis of Pd/CuO nanoparticles by Theobroma cacao L. seeds extract and their catalytic performance for the reduction of 4-nitrophenol and phosphine-free Heck coupling reaction under aerobic conditions, *J. Colloid Interface Sci.*, 2015, **448**, 106–113.

99 A. A. Kassem, H. N. Abdelhamid, D. M. Fouad and S. A. Ibrahim, Catalytic reduction of 4-nitrophenol using copper terephthalate frameworks and CuO@C composite, *J. Environ. Chem. Eng.*, 2021, **9**(1), 104401.

100 X. Zhang, X. He, Z. Kang, M. Cui, D. P. Yang and R. Luque, Waste Eggshell-Derived Dual-Functional CuO/ZnO/Eggshell Nanocomposites: (Photo)catalytic Reduction and Bacterial Inactivation, *ACS Sustainable Chem. Eng.*, 2019, **7**(18), 15762–15771.

101 K. Sahu, B. Satpati, R. Singhal and S. Mohapatra, Enhanced catalytic activity of CuO/Cu2O hybrid nanowires for reduction of 4-nitrophenol in water, *J. Phys. Chem. Solids*, 2020, **136**, 109143.

102 A. G. Bekru, O. A. Zelekew, D. M. Andoshe, F. K. Sabir and R. Eswaramoorthy, Microwave-assisted synthesis of CuO nanoparticles using cordia africana Lam. leaf extract for 4-nitrophenol reduction, *J. Nanotechnol.*, 2021, 581621.